ACS OMEGA

Open Access

http://pubs.acs.org/journal/acsodf

Article

Apoptotic Potential and Antitumor Efficacy of Trilliumoside A: A New Steroidal Saponin Isolated from Rhizomes of *Trillium govanianum*

Misbah Tabassum,[#] Bashir Ahmad Lone,[#] Mudasir Nazir Bhat, Anil Bhushan, Nagma Banjare, Esteban Manrique, Prasoon Gupta, Dilip M. Mondhe,* and Prem N. Gupta*

Cite This: *ACS Omega* 2023, 8, 31914−31927

Read Online

ACCESS | Metrics & More | Article Recommendations | Supporting Information

ABSTRACT: Natural product-derived molecules exhibit potential as anticancer agents. Trilliumoside A, a new steroidal saponin, was obtained from rhizomes of *Trillium govanianum*, and its anticancer activity was investigated in the presented study. Trilliumoside A was investigated in a panel of cell lines, and it exhibited promising cytotoxic activity on the A549 cells (human lung cancer cells) with an IC_{50} of 1.83 μM. The mechanism of cell death induced by Trilliumoside A in A549 cells and its anticancer potential in murine tumor models (EAC and EAT) were presented in the current research. Trilliumoside A was found to induce apoptosis in A549 cells by increasing the expression of various apoptotic proteins, such as Bax, Puma, cytochrome C, cleaved PARP, and cleaved caspase 3. Additionally, Trilliumoside A regulates the expression of p53, CDK2, and Cyclin A by decreasing the mitochondrial membrane potential, elevating reactive oxygen species, and stopping the growth of A549 cells in the synthesis phase (S) of the cell cycle. Trilliumoside A showed a considerable reduction in the tumor volume, the amount of ascitic fluid, and the total cell number without affecting the body weight of animals. Our results demonstrate that Trilliumoside A inhibits the proliferation of human lung cancer cells by inducing DNA damage, arresting the cell cycle, and activating the mitochondrial signaling pathway. The study demonstrated the potential of Trilliumoside A as a potential anticancer agent.

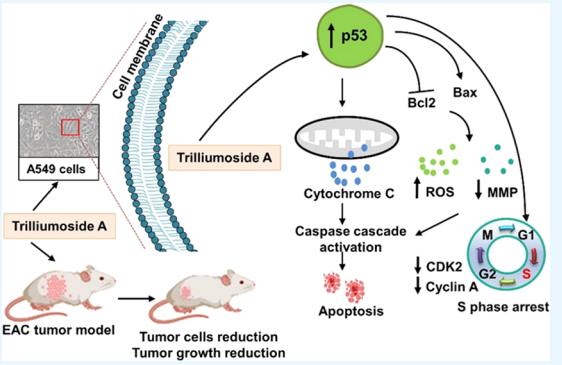

1. INTRODUCTION

Unregulated and uncontrolled division of cells in a body leads to one of the deadliest diseases humanity has ever witnessed; modern science calls it cancer, a word derived from concrum, a Latin word meaning crab. Among all the cancers, lung cancer is considered the second most diagnosed cancer, contributing to the highest mortality.[1,2] Lung cancer contributes 23% of the total cancer-related deaths in humans all over the world.[3] Lung cancer is one of the common cancers all over the globe due to rapid progression, high incidence, and poor prognosis.[4,5] Small-cell lung carcinoma (SCLC) and non-small cell lung carcinoma (NSCLC) are the two types of lung cancer that make up 85% of the cases. NSCLC is regarded as a prominent and prevalent form of cancer.[3,6] In the Asian subcontinent, lung cancer exists as the potential reason for deaths and reduces the 5-year survival ratio by less than 15%.[7] Lung cancer is also growing steadily in developing countries due to the adoption of western culture, alcohol, sedentary life style, consumption of tobacco, and obesity.[8] Due to tumor diversity, limited understanding of cancer biology, development of reluctance to therapies, and late disease presentation become the leading causes of high mortality in patients with lung cancer.[9] The process of apoptosis through programmed cell death occurs naturally. Drug-induced apoptosis is crucial in the treatment of cancer.[10] The mitochondria apoptosis is the best-known pathway for cancer treatment acting by altering the mitochondrial membrane permeability by releasing the apoptosis vital substances, activating Bcl-2 family members[11] and downstream caspase proteins.[12]

At present, chemotherapy is used as the potential tool for the curing of lung cancer. The conventional cancer therapies for enhanced survival and better quality of living for patients affected are still limited and associated with various limitations.[13] The lipophilic nature and usage of higher doses of chemotherapeutics require surfactant-based solubilization to enhance the systemic drug availability. In addition, due to the first-pass metabolism, the oral dosage of cancer chemotherapeutics is restricted.[14−16] The spreading of cancer is

Received: May 24, 2023
Accepted: August 8, 2023
Published: August 23, 2023

rapid depending on the progression and proliferation of cell division.[17] The present antitumor chemical drugs show some consequential side effects[18,19] due to which the continuous exploration of new chemical treatment with less side effects is vital. For cancer treatment, various chemotherapeutics of plants are being used. These chemotherapeutics showed their action via different mechanisms of action.[20] The natural product-derived molecules that showed anticancer properties may belong to any of the categories of molecules such as alkaloids, diterpenes, etc.[21] Natural product-derived molecules exhibited great potential for the treatment of cancer, and there are a number of molecules including paclitaxel, vincristine, vinblastine, bleomycin, zingiberene, and trabectedin, which have been explored for the management of cancer.[22]

We have reported Trilliumoside A, a natural product isolated for the first time from the rhizome of the *Trillium govanianum* Wall. ex D. Don.[23] The plant is one of the best potential medicinal herbs with a lot of therapeutic value.[24] The previous literature suggested that the plant has cytotoxic properties on the basis of how the plant was used for the treatment of lung, liver, and breast cancers.[25] In this study, we found that Trilliumoside A showed anticancer activity against the lung cancer by activation of mitochondrial signaling pathways and inducing DNA damage.

2. METHODOLOGY

2.1. Reagents, Chemicals, and Antibodies. Ammonium per sulfate, acrylamide, bromophenol blue, Coomassie Brilliant Blue, Triton X100, N, *N*-methylene bisacrylamide, Trizma base, EDTA, phosphate-buffered saline (PBS), sodium bicarbonate, β mercaptoethanol, trypsin, RIPA buffer, rhodamine 123 (Rh123), SRB dye, TEMED, DCFHDA, RPMI 1640 medium, DMEM, DMSO, HEPES, 5 fluorouracil (5FU), phenyl methyl sulfonyl fluoride (PMSF), protease inhibitor cocktail, bovine serum albumin (BSA), Annexin V- FITC kit, and propidium iodide (PI) were purchased from Sigma-Aldrich Co. Fetal bovine serum (FBS) and penicillin−streptomycin solution were procured from GIBCO Invitrogen Corporation. Methanol, glycerol, and glycine were obtained from Himedia Laboratories, Dindori, India; the chemiluminescent horseradish peroxidase (HRP) substrate was obtained from Millipore Corporation. Procaspase antibody sampler kit, Cytochrome C, Puma, anti-actin antibody, anti-Bax, and anti-Bcl2 were obtained from Cell Signaling Technologies (CST). The CL-XPosure film and protein ladder have been purchased from Thermo Scientific (Rockford).

2.2. Cell Culture and Optimum Growth Conditions. Human cancer cell lines including colon cancer (HCT-116, SW-620), lung cancer (A-549, HOP-62), pancreatic cancer (MiaPaCa-2), breast cancer (MCF-7, MDA-MB 231), prostate cancer (PC-3), and neuroblastoma (SH-SY5Y) were obtained from the National Cancer Institute (NCI). From the European Collection of Authenticated Cell Cultures (ECACC), the non-tumor human breast epithelial cell line FR2 was obtained. The cell lines are maintained and passed serially in accordance with the literature.[26] RPMI-1640 and DMEM complete growth media supplemented with 10% fetal bovine serum, 100 mg/mL streptomycin, and 100 units/mL penicillin were used to grow the human cancer cell lines in tissue culture flasks at 37 °C, 5% CO_2, and 95% RH.

2.3. Extraction and Isolation of Trilliumoside A. Trilliumoside A was isolated from shade-dried rhizomes of the *T. govanianum* (1.9 kg, 20% aq. MeOH) extract (229.44 g) and subjected to purification using HP-20 resin as the reverse phase in an open glass column chromatograph; the column was eluted with decreasing polarity of the (water/methanol) solvent system. 250 mL volume of each collected flask was concentrated using a rotavapor. On their similarity in the TLC profile, 20 sub-fractions (HA-01-HA-20) were obtained. With sub-fraction F-1D (1.2 g) on further purification using reverse-phase column chromatography, HP-20SS dianion exchange resin was used as a stationary phase and water:methanol as a solvent system (0.5:9.5−8.5:2.5) 25 mL collected in 50 mL tubes; on the basis of TLC profile fractions (6.5:3.5), (8.5:2.5) afforded **compound 1** (27 mg) as a dark-brown crystalline solid. The isolated compound was characterized by 1D and 2D NMR, LC/MS, and HR/MS; HPLC purity of isolated compounds used for all biological assays was >98%. Its molecular formula was determined to be $C_{51}H_{85}O_{23}$, by LC/MS data at (m/z 1064.13 $[M + H]^+$) (calcd for $C_{51}H_{85}O_{23}^+$,1064.1911), together with its NMR data.^{1}H NMR (400 MHz, MeOD) δ 5.38 (s, 1H), 5.19 (s, 1H), 4.83 (s, 1H), 4.49 (d, J = 7.8 Hz, 1H), 4.23 (d, J = 7.8 Hz, 1H), 4.16−4.07 (m, 2H), 3.93 (d, J = 2.9 Hz, 1H), 3.88−3.82 (m, 2H), 3.78 (s, 1H), 3.68−3.63 (m, 3H), 3.63−3.60 (m, 2H), 3.59 (s, 1H), 3.43−3.35 (m, 5H), 3.34 (s, 2H), 3.26 (s, 1H), 3.18 (q, J = 7.3 Hz, 7H), 2.44 (d, J = 9.8 Hz, 1H), 2.31−2.20 (m, 2H), 2.01 (d, J = 8.1 Hz, 2H), 1.90 (s, 2H), 1.72−1.50 (m, 6H), 1.32 (s, 2H), 1.30 (s, 3H), 1.28 (s, 3H), 1.26 (s, 1H), 1.24 (s, 3H), 1.23 (s, 1H), 1.17 (t, J = 7.0 Hz, 2H), 1.04 (s, 3H), 0.92 (m, 6H), 0.84 (s, 2H).^{13}C NMR (100 MHz, MeOD) δ38.67 (C-1), 30.55 (C-2), 79.45 (C-3), 39.58 (C-4), 141.95(C-5), 122.75(C-6), 32.33(C-7), 33.18(C-8), 51.52(C-9), 38.01 (C-10), 21.18 (C-11),30.55 (C-12), 46.12(C-13), 53.92(C-14), 33.01(C-15), 90.89(C-16), 91.62(C-17), 17.50(C-18), 20.10(C-19), 50.00 (C-20), 9.87(C-21), 112.46(C-22), 36.88(C-23), 28.55(C-24), 35.07(C-25), 58.43(C-26), 76.11(C-27).3-*O*-Glcδ 100.50 (C-1′), 77.95 (C-2′), 78.16 (C-3′), 79.92 (C-4′), 76.69 (C-5′), 62.00 (C-6′), 2-*O*-Rha103.4 (C-1″), 71.75 (C-2″), 73.98 (C-3″), 79.32 (C-4″), 69.86 (C-5″), 18.14 (C-6″), 4-*O*-Rha102.2(C-1‴), 72.50 (C- 2‴), 72.25 (C-3″)′, 73.81 (C-4″)′, 70.72 (C-5‴), 18.02 (C-6‴), 26-*O*-Glc-104.66 (C-1⁗), 75.24 (C-2⁗), 78.19 (C-3⁗), 72.40 (C-4⁗), 78.04 (C-5⁗), 62.83 (C-6⁗).[23]

2.4. Cell Viability Screening in Human Cancer Cell Lines Using SRB Assay under In Vitro Conditions. In 96-well flat-bottom plates, the optimal cell density per well was seeded in order to perform the SRB assay according to a previous protocol.[27] Human cancer cell lines namely colon cancer (SW-620, HCT-116), lung cancer (A-549, HOP-62), prostate cancer (PC-3), breast cancer (MCF-7, MDA-MB 231), pancreatic cancer (MiaPaCa-2), and neuroblastoma (SH-SY5Y) were seeded at 100 μL/well in a 96-well plate. The cells were exposed to test substances at varying concentrations (0.5, 1, 2.5, 5, 10, and 20 μM) and the plates were incubated for 48 h. Furthermore, ice-cold TCA was used to fix cells. Additionally, cells were fixed for one hour at 4 °C with ice-cold TCA. The plates were given three water rinses after 1 h and then left to air-dry. In the following step, 100 μL of 0.4% SRB dye was applied, and plates were left at room temperature. After that, plates were washed once with 1% acetic acid and three times with water to remove the unbound SRB. The bound dye was solubilized after drying at room temperature by adding 100 μL of 10 mM Tris buffer (pH-10.4) to each well. To dissolve the protein-bound dye, the plates were shaken for

https://doi.org/10.1021/acsomega.3c03649
ACS Omega 2023, 8, 31914−31927

5 min. OD was determined at 540 nm in a microplate reader (Thermo Scientific) and cell viability was calculated.

2.5. Morphological Studies Using 4,6-Diamidino-2-phenylindole (DAPI) Staining and Bright Field Microscopy. DAPI labeling was used to examine apoptosis in A-549. Trilliumoside A was incubated with the cells for 48 h at doses of 1, 2, 4, and 6 μM. Cells serving as positive controls received camptothecin (CPT) at a concentration of 0.25 μM. After 48 h of incubation, cells were washed with PBS. At 4 °C, cells were fixed in a 3:1 methanol/acetic acid fixing solution. To identify the nuclear alterations, cells were first cleaned with PBS before being stained for 30 min in the dark with 10 μmol/L working solution of DAPI. Cells were washed with PBS after 30 min of treatment, and then, under a fluorescence microscope, apoptosis-related nuclear morphological alterations were seen.[28,29] Morphological investigation following exposure with Trilliumoside A was also investigated using bright field microscopy.

2.6. Examination of the A549 Cell Surface Using Scanning Electron Microscopy (SEM). To examine the effect of Trilliumoside A on the cell morphology of A549 cells, scanning electron microscopy was used. Cells were treated with four different doses of Trilliumoside A for this test, plated on coverslips, and fixed with 2.5% glutaraldehyde for 24 h. Following the incubation, the samples were washed with PBS and fixed for 4 h at 4 °C in a solution of 1% osmium tetroxide. We used graded ethanol solutions to dehydrate fixed cells. Hexamethyldisilazane was used to dry cells at their critical point. The specimens received a gold sputter coating.[29] Samples were analyzed using a scanning electron microscope for any structural alterations post Trilliumoside A treatment.

2.7. Examination of Cell Apoptosis Using Acridine Orange−Ethidium Bromide (AO-EtBr) Staining. A549 cells were seeded in 6 wells for an overnight period at a density of 1×10^4 cells per well. After 24 h of incubation, cells were treated with Trilliumoside A at 1, 2, 4, and 6 μM concentrations for 48 h. The dual dye mixture of 100 μg/mL AO and 100 μg/mL EtBr in PBS[30] was added after the cells had been rinsed with ice-cold 1× PBS, and images were taken using an Olympus IX53 microscope.

2.8. Apoptosis and Necrosis Assessment by Annexin V-Fluorescein Isothiocyante (FITC)/PI Dual Staining. Using a flow cytometer, an analysis of Annexin V FITC was performed in an effort to comprehend how Trilliumoside A causes the induction of apoptosis. A-549 cells were plated in six-well plates at a density of 1×10^5 cells per well. Trilliumoside A was administered to cells at concentrations of 1, 2, 4, and 6 μM. Following a 48 h incubation period, cells were collected, labeled with Annexin V (a phosphatidylserine-binding protein) in conjunction with FITC dye, and analyzed using a BD FACS system.[29,31]

2.9. Scratch Assay. Scratch assay is an in vitro assay, which was used to measure the migration and proliferation of mammalian cells after treatment with cytotoxic drugs.[31,32] A549 cells were allowed to grow in a 6-well plate until a monolayer of cells is formed, and then, a scratch in a horizontal line is made in the monolayer with a sterile microtip. Incubation of cells was done with different concentrations of Trilliumoside A for 48 h. The scratched area was photographed at both 0 and 48 h, and the percentage of wound closure or gap was calculated using the formula

$$\%\ \text{wound closure} = \frac{\text{wound area at 0 h}}{\text{wound area at 48 h}} \times 100$$

2.10. Colony Forming Assay. Colony formation assay is a cell survival assay done in in vitro conditions, which is based on the fact that a single cell divides and forms colonies when provided with optimal conditions to grow. A group of cells consisting of 50 or more cells is said to be a colony. This assay helps determine the loss of reproductive ability of a cell when exposed to various external agents such as radiations and cytotoxic drugs. Only fractions of treated cells retain this ability of producing colonies. Cells were grown in a tissue culture-treated six-well plate having a density of 3×10^5 cells per well. Trilliumoside A was given to the cells for 48 h at concentrations of 1, 2, 4, and 6 μM. Following the treatment with the test compound, cells were harvested and subjected to PBS washing thrice and re-seeded 1000 cells/well for two weeks. After the prescribed period, the visible colonies were fixed with 4% paraformaldehyde for 30 min and staining of fixed colonies was done with crystal violet dye for 20 min.[33] Manual counting of the colonies or using Image J software was done followed by photography. The percentage of colonies formed was estimated using the following formula

$$\text{colony formation rate}(\%) = \frac{\text{number of colonies in treatment group}}{\text{number of colonies in control group}} \times 100$$

2.11. Assessment of Mitochondrial Membrane Depolarization. The cytoplasmic release of apoptogenic stimuli causes the loss of mitochondrial membrane potential, which results in cell death. 1×10^5 cells were sown into each well of a six-well plate, and the cells were left in the incubator overnight to develop their morphology. Cells were treated with Trilliumoside A at concentrations of 1, 2, 4, and 6 μM along with camptothecin as a positive control at a concentration of 0.25 μM, and the plates were left to incubate for 48 h. PBS washing was given twice, and 1 mL of 200 nM of Rhodamine-123 dye was added to each well and the plate was incubated for 15 min so as to allow the cells to take up the dye. After 15 min, the wells were washed with PBS thrice and 1 mL of incomplete media was added to each well and images were taken under a fluorescence microscope.[34,35] The loss of mitochondrial membrane potential was additionally investigated using Mitotracker red dye.

2.12. Immunocytochemistry of A549 Cells. A549 cells were treated with the Trilliumoside A at the concentrations of 1, 2, 4, and 6 μM. Immunocytochemistry was performed using the previously reported protocol.[36] Following 48 h of incubation, the cells were washed with PBS. After that, fixation of cells was done with 4% paraformaldehyde for 15 min at room temperature. Cell permeablility was achieved with 0.1% Triton X-100 in PBS solution for 5 min and occluded with 1% BSA for 1 h. The incubation of cells was done with specific primary antibodies for 1 h and washed thrice with PBS to detect cytochrome c expression/localization. The cells were then incubated with Alexa Fluor 488 combined with the secondary antibody (for cytochrome c) for 1 h. After incubation, the cells were washed and stained with DAPI and examined using a fluorescence microscope Olympus IX53.

2.13. Determination of Intracellular Peroxides (ROS Assay). The main sign that a cell is going through apoptosis shows an increase in the production of reactive oxygen species.

https://doi.org/10.1021/acsomega.3c03649
ACS Omega 2023, 8, 31914−31927

1×10^5 cells were seeded into each well of a six-well plate, and the cells were left in the incubator overnight to develop their morphology. Cells were exposed to Trilliumoside A at doses of 1, 2, 4, and 6 μM. Cells were rinsed with PBS after 48 h of incubation, and then, 10 μmol/L DCFDA dye was added to each well for 20 min. Once more, PBS washing was given, and a fluorescence microscope was used to view images. Here, H_2O_2 was used as a positive control.[35]

2.14. Flow Cytometric Assessment of Cell Cycle Phases. Incubation of A-549 cells was done with Trilliumoside A at different concentrations for 48 h. Cells were washed with PBS and fixed in 70% ethanol overnight. Cells were digested with RNase (0.1 mg/mL) for 90 min at 37 °C and then stained with PI (50 μg/mL).[34] Using a flow cytometer, cells were analyzed. BD FACS calibre was used to determine the final outcome of DNA distribution in distinct cell cycle phases.[37] FlowJo software, version 10.8.1 (BD Biosciences), was used to analyze the data.

2.15. Western Blot Analysis. A549 cells were treated with Trilliumoside A at different concentrations for 48 h. Cells were washed with PBS, pelleted using centrifugation, and then resuspended for 45 min in an ice-cold RIPA buffer solution with a protease inhibitor cocktail. At 4 °C, cell lysates were centrifuged for 20 min at 12 000 rpm. Laemmli buffer was then used to solubilize the cell lysates.[38] The lysates were loaded, separated by sodium dodecyl sulfate−poly(acrylamide gel) electrophoresis at 70 V for 3 h, and then transferred to the poly(vinylidene diflouride) (PVDF) membrane at 100 V for 2 h. Proteins in PVDF were blocked by using 5% non-fat skim milk (in tris buffer saline supplemented with 0.1% Tween-20) for 1 h. The membrane was incubated with the primary antibody for a whole night at 4 °C and then with the secondary antibody combined with HRP for an additional hour. The protein blots were washed three times with TBST for five minutes. To find the protein signal trapped on an X-ray film, the ECL plus chemiluminescent (HRP) substrate was utilized,[39] and Image J software was used for the densitometry.

2.16. In Vivo Anticancer Activity. The anticancer potential of Trilliumoside A was examined in using the Ehrlich ascites carcinoma (EAC) and Ehrlich solid tumor (EAT) models. The in vivo animal experimentation protocols were approved by the Institutional Animal Ethics Committee (IAEC). On day 0, 1×10^7cells were injected into each animal intramuscularly (right thigh) and intraperitoneally (i.p.) to develop the EAT and EAC models, respectively.[39] On the first day, the mice were randomly assigned to different groups and given doses of Trilliumoside A intraperitoneally at 25, 50, and 75 mg/kg for nine days. In the ascites and solid tumor models, 5FU was used as a positive control with doses of 20 and 22 mg/kg, respectively. Animals were sacrificed on day 12, and ascitic fluid was collected from each mouse's peritoneum to measure tumor growth.[39] Based on the total number of tumor cells present in the peritoneal cavity of the treated and untreated mice, the percentage of tumor growth inhibition was computed.[40] Tumor dimensions for the EAT (solid) model were measured using a vernier calliper on days 9 and 13[34] and the formula shown below was used to determine the tumor's weight

$$\text{tumour weight(mg)} = \frac{\text{length(mm)} \times [\text{breadth(mm)}]^2}{2}$$

2.17. Statistical Analysis. Results are shown as mean standard deviation (SD) in this study. One-way analysis of variance (ANOVA), followed by the Tukey or Bonferroni post-test, was used to analyze the data in Image J and GraphPad Prism (version 5). Values with significance levels of $^*p < 0.05$, $^{**}p < 0.01$, and $^{***}p < 0.001$ were used.

3. RESULTS

3.1. Screening of Isolated Compounds for Cytotoxicity. Trilliumoside A and other pure isolated compounds were screened against different cancer cell lines for cytotoxic activity (Table S1). The IC_{50} values of Trilliumoside A against different cancer cell lines are shown in Table 1. Based on initial screening among all the isolated compounds, Trilliumoside A was selected for further mechanistic studies. Trilliumoside A has been isolated as a brownish solid. Its molecular formula $C_{51}H_{85}O_{23}$ was deduced by LC/ESI/MS data; (m/z 1064.1219 $[M+H]^+$ (calcd. for $C_{51}H_{84}O_{23}$, 1063.13), along with its ^1H,^{13}C and 2D NMR data. The structure of Trilliumoside A is shown in Figure 1A. Trilliumoside A has the lowest half-maximal inhibitory concentration and the maximum cytotoxicity against all cancer cell lines with IC_{50} values of 2.91 and 1.85 μmol/L against colon (HCT-116 and SW−62 0), 1.83 and 1.92 μmol/L against lung (A549,HOP-62), 3.18 μmol/L prostate (PC3), 1.94 μmol/L pancreas (MiaPaCa-2), 4.40, 1.90 μmol/L breast (MCF-7 and MDA-MB-231), 2.43 μmol/L neuroblastoma (SH-SY5Y), and 13.75 μmol/L normal epithelial cell (FR2) lines, as treated with this compound for 48 h. The analysis revealed that the IC_{50} value of Trilliumoside A was more than sevenfold higher against the normal breast epithelial cell line FR-2 than the lung cancer cell line A549, thereby indicating a greater selectivity index (Table S2).

Table 1. IC_{50} Values (μM) of Trilliumoside A and Camptothecin (CPT) against Various Cell Lines Using Sulforhodamine B (SRB) Assay

cell line	Trilliumoside A	CPT
	IC_{50} (μM)	
A549	1.83 ± 0.54	0.030 ± 0.04
HCT-116	2.91 ± 0.50	0.160 ± 0.23
MCF-7	4.40 ± 0.33	0.147 ± 0.13
MDA-MB 231	1.90 ± 0.26	0.125 ± 0.03
MIAPACA-2	1.94 ± 0.24	0.060 ± 0.02
SW-620	1.85 ± 0.52	0.093 ± 0.03
SHSY5Y	2.43 ± 0.32	
PC-3	3.18 ± 0.37	0.170 ± 0.03
HOP-62	1.92 ± 0.62	0.065 ± 0.04
EAC	8.45 ± 0.87	
FR2	13.75 ± 0.42	<0.01 ± 0.001

3.2. Trilliumoside A Selectivity toward A549 Cells over Time. Trilliumoside A's in vitro anticancer activity against A549 cell lines was examined, and the IC_{50} values of Trilliumoside A at 6, 12, 24, and 48 h (Figure 1B and Table S3) were observed to be 24.95, 16, 8.35, and 1.83 μM for A549. The results showed that the antiproliferation effect of Trilliumoside A increases in a time-dependent manner. The effective time period was found to be 48 h, and therefore, all the mechanistic studies were carried out at 48 h time point.

3.3. Trilliumoside A Induces Apoptosis of A549 Cells (DAPI Staining). Apoptosis induced by the cytotoxic effect of Trilliumoside A was investigated in A549 cells. Apoptotic

https://doi.org/10.1021/acsomega.3c03649
ACS Omega 2023, 8, 31914−31927

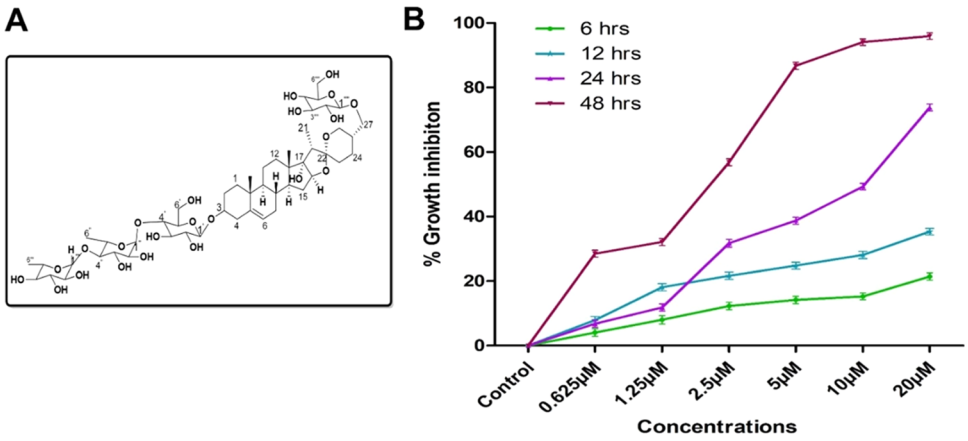

Figure 1. (A) Structure of Trilliumoside A. (B) Graph represents time-dependent antiproliferative activity of Trilliumoside A against A549 cancer cells detetmined by SRB assay.

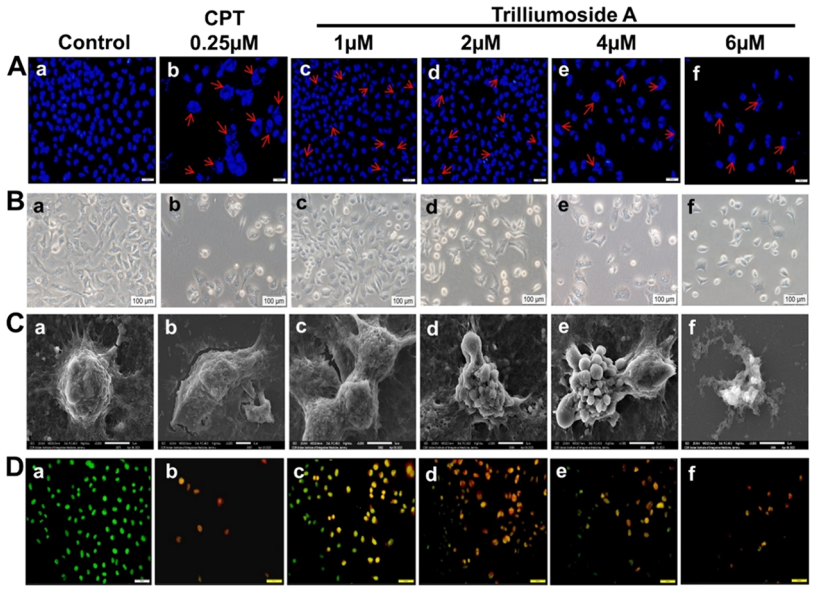

Figure 2. (A) Trilliumoside A induced apoptosis in A549 cells. Fluorescence microscopic images of DAPI (4,6 diamidine-2 phenylindole)-stained A549 cells. Treatment with Trilliumoside A for 48 h exhibited concentration-dependent nuclear morphological changes, including nuclear fragmentation, nuclear condensation, and membrane blebbing. (B) Bright-field microscopic study of A549 cells. After being exposed to Trilliumoside A for 48 h, cells exhibited the morphological alterations associated with apoptosis, including roundness, decreased cell quantity, and rough surface. (C) Scanning electron microscopy of Trilliumoside A-treated cells displayed the surface ultrastructure of A549 cells. SEM analysis displaying apoptotic cell death hallmarks, including smoothing of the plasma membrane, disappearance of micro villi, membrane blebbing, and production of apoptotic bodies. (D) Trilliumoside A induces cell death in A549 cells. After being incubated with Trilliumoside A for 48 h, A549 cells exhibit acridine orange−ethidium bromide staining. Camptothecin (CPT) was the positive control. Indicators of concentration-based activation of cell death included increased orange and red fluorescence.

changes were revealed by different studies such as fluorescence and bright -field microscopy studies, by using nuclear staining of the DAPI (4,6 diamidine-2 phenylindole) dye. Numerous abnormalities or morphological changes such as membrane flattening, blebbing, enlarged, and uneven patterns in the cell shape with some projections were observed in various Trilliumoside A-treated cells and were compared with untreated cells. DAPI staining in Trilliumoside A-treated cells also revealed that A549 cells had died as a result of their nucleus becoming condensed, fragmented, and distorted, and the production of apoptotic bodies was observed. In comparison to the control, these alterations were more prevalent in cells treated with Trilliumoside A and the positive control camptothecin (Figure 2A). Also, bright-field microscopic study of A549 cells following exposure to Trilliumoside A for 48 h showed morphological alterations associated with apoptosis, including roundness, decreased cell quantity, and rough surface (Figure 2B).

3.4. Surface Ultrastructural Studies. A549 cells upon treatment with Trilliumoside A showed the formation of apoptotic bodies as seen in the images obtained with the help of SEM (Figure 2C). A549 cells showed the characteristic features of programmed cell death including loss of microvilli, blebbing, and condensation. Control or untreated cells exhibited characteristics of typical cancer cells, including mature shape and unaltered microvilli.

3.5. Acridine Orange−Ethidium Bromide (AO-EtBr) Staining. Cancer drugs usually induced apoptosis in cancer cells and necrosis in some cases. Apoptosis is a widely studied cell death pathway mediated by complexes. Qualitative

https://doi.org/10.1021/acsomega.3c03649
ACS Omega 2023, 8, 31914−31927

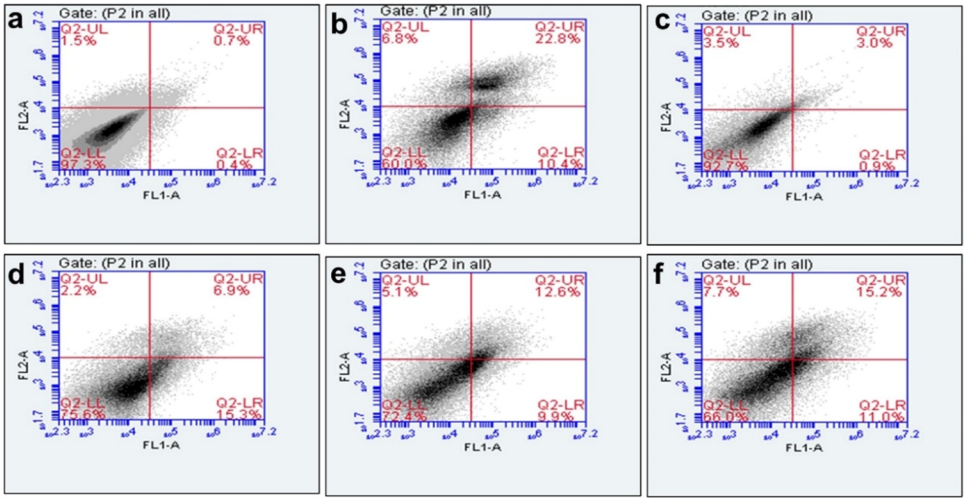

Figure 3. Trilliumoside A-induced apoptosis analysis employing flow cytometry and Annexin V-FITC. As a positive control, CPT was used. Nontreated and treatment groups include the control group, CPT (0.25 μM), Trilliumoside A (1 μM), Trilliumoside A (2 μM), Trilliumoside A (4 μM), and Trilliumoside A (6 μM) and are denoted by a–f, respectively.

evaluation of apoptosis was done by acridine orange–ethidium bromide (AO-EtBr) staining to evaluate apoptosis in the treated cancer cells. After staining, difference among treated and nontreated cells will appear on the basis of the color of fluorescence like uniform green fluorescence is displayed by live cells, and orange and red fluorescence shows apoptotic and dead cells, respectively. The cytological reaction of A549 cells after treatment with Trilliumoside A was done using AO/EtBr double staining. As shown in Figure 2D, control cells (untreated) exhibited uniform light-green fluorescence, indicating that all cells were viable. In contrast, after being exposed to Trilliumoside A at various doses for 48 h, an increase in orange fluorescence was observed due to increased apoptotic cells. Cells showed relatively higher death as the concentration of Trilliumoside A increased.

3.6. Estimation of Trilliumoside A-Induced Cellular Apoptosis (Annexin V-FITC/PI). A549 cells displayed an increase in early apoptotic cells from 0.4 to 15.3% at 2 μM concentration, while late apoptotic cells were increased from 0.7 to 3%, 6.9, 12.6, and 15.2% at a concentration of 1, 2, 4, and 6 μM (Figure 3). The positive control used is camptothecin (0.25 μM), indicating an early and late apoptotic population of 10.4 and 22.8%, respectively.

3.7. Trilliumoside A Inhibits A549 Cell Ability to Migrate and Invade. The effect of Trilliumoside A was investigated by cell scratch assay to inspect the invasive prospects and migration of cells. Trilliumoside A decreases the migration of A549 cells toward the margins of the wound by creating a small amount of gap closure. On the contrast, proficient gap closure was seen between the cells in untreated control cells. Trilliumoside A was used in A549 cells at concentrations of 1, 2, 4, and 6 μmol/L, and the percentage of wound closure was shown to have decreased from 60.27% in the control to 29.5, 25.38, 9.76, and 5.9% in treated cells, respectively (Figure 4A,D).

3.8. Colony Assay. Trilliumoside A's antiproliferative effects were further investigated using a colony formation assay, in which A549 cells were exposed to different concentrations (1, 2, 4, and 6 μmol/L) for 48 h. The results showed that Trilliumoside A brings forth the irreversible growth arrest capability, which in turn leads to a decrease in the number of colonies formed as compared to control cells (Figure 4B,C,E).

3.9. Effect of Trilliumoside A on Mitochondrial Membrane Integrity and Release of Cytochrome C in A549 Lung Cancer Cells. Treatment of A549 cells with varying dosages of Trilliumoside A for 48 h resulted in loss of mitochondrial membrane integrity and other forms of malfunction. The cells were seen under a fluorescence microscope labeled with Rh-123. The control had the strongest fluorescence impact (100%) as shown by Figure 5A,B,D,E. When compared to the control, cells treated with Trilliumoside A showed decreasing fluorescence intensities of 55, 18.33, 11.48, and 5.4% at 1, 2, 4, and 6 μmol/L, respectively ($P < 0.05$). This demonstrates that the depolarization of the mitochondria in A549 cells was apparently induced by Trilliumoside A, resulting in enhanced loss of MMP ($\Delta\Psi$ m). Similarly, MMP of A549 cells dosed with camptothecin turned down to 10%. The cytosolic release of cytochrome c was examined using western blot analysis in order to establish the loss of MMP and the breakdown of the mitochondrial membrane. These tests revealed that Trilliumoside A enhanced the release of cytochrome c in A549 cells (Figure 5F,G).

3.10. Trilliumoside A Causes the Release of Cytochrome C (Immunocytochemistry). A549 cells treated with Trilliumoside A show more release of cytochrome c as compared to the untreated cells. Figure 5C depicts diffused staining of treated cells and undispersed staining of control cells, thereby confirming the movement of cytochrome C from the mitochondria to the cytoplasm.

3.11. Generation of ROS in A549 Lung Cancer Cells. Reactive oxygen species (ROS) are primarily produced by the mitochondria in mammalian cells, and ROS production is frequently triggered by MMP deficiency. Therefore, we investigated whether the MMP reduction brought on by Trilliumoside A has an effect on ROS production in A549 cells. We determined the degree of ROS production in A549 cells using the DCFH -DA fluorescent probe for ROS. Fluorescence microscopy analysis showed 30, 65, 80, and 95% elevation of ROS at 1, 2, 4, and 6 μM concentrations of Trilliumoside A, respectively, as compared to the negative control (Figure 6A,B).

https://doi.org/10.1021/acsomega.3c03649
ACS Omega 2023, 8, 31914–31927

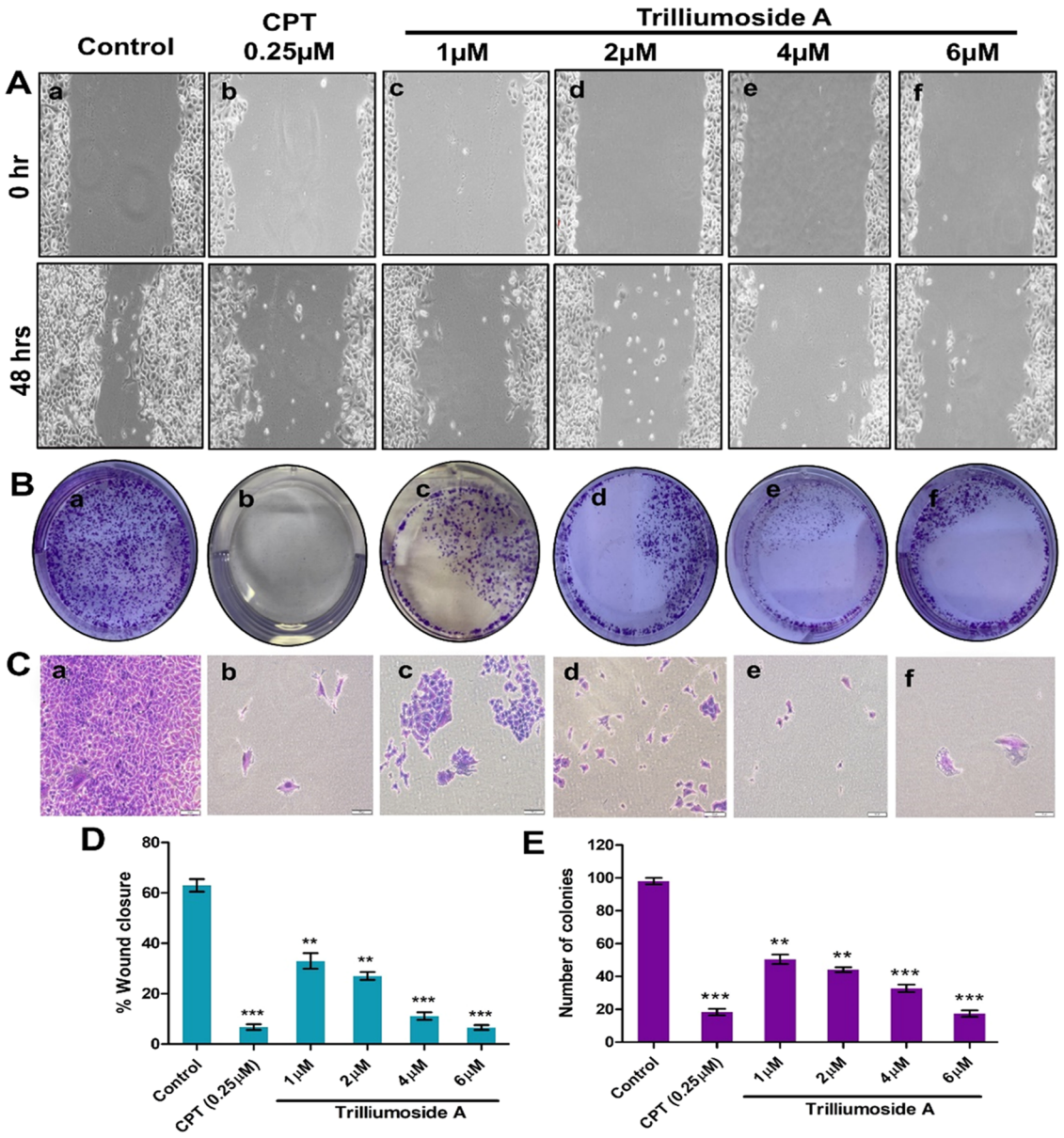

Figure 4. (A) In vitro scratch assay was performed on A549 cells. Phase contrast microscopy was used to capture images at 0 and 48 h. The migration rate was determined by quantifying the gap left by the scratch. Trilliumoside A significantly decreases the migratory of A549 cells in a concentration-dependent manner; in contrast, the control (untreated) well gap was almost filled in 48 h. (B) Trilliumoside A inhibits colony formation in A549 cells. The images from the clonogenic experiment on the A549 cell line showed the inability of single cells to multiply and grow into a colony after being treated with Trilliumoside A. (C) Microscopic images of a single colony at different treatments of Trilliumoside A at 20× magnification showing a less number of colonies with reduced size were formed in contrast to the negative control well. (D) Graph showing the % wound closure decreases as the concentration of Trilliumoside A increases. (E) Graph showing the number of colonies reduced with elevated levels in a drug concentration of Trilliumoside A. Data were expressed as mean ± SD, $^{**}P < 0.01$ and $^{***}P < 0.001$ represent significant difference compared to the control.

3.12. Effects of Trilliumoside A on the Cell Cycle. Flow cytometric analysis was used to estimate the DNA phase distribution of Trilliumoside A-treated A549 cells. On Trilliumoside A treatment, the percentages of the G1 phase population were 69.2, 64.9, 57.6, and 50.2% and those of the S phase population were 21.3, 28.5, 31.6, and 37.9% at 1, 2, 4, and 6 μM concentrations, respectively. However, little changes were noted in the G2 phase as shown in Figure 6C,D. Camptothecin was used as a positive control with G1, S, and G2 populations of 2.17, 63.5, and 34.5% at 0.25 μM concentration.

3.13. Trilliumoside A Causes Apoptosis in A549 Cells through the Intrinsic Apoptotic Pathway. We investigated how Trilliumoside A affected the production of different caspase proteins because the caspase cascade is thought to be one of the most important aspects of programmed cell death. The results revealed that Trilliumoside A-treated cells experience enhanced activity of caspases as the cleavage of caspase-3 and -9 got increased in a dose-dependent fashion, on comparison with control or untreated cells. Trilliumoside A activated PARP protein also by cleaving it, initiating the cell death via intrinsic mode of apoptosis [Figure 7Aa, Ba]. As a positive control, camptothecin was used, and as

https://doi.org/10.1021/acsomega.3c03649
ACS Omega 2023, 8, 31914−31927

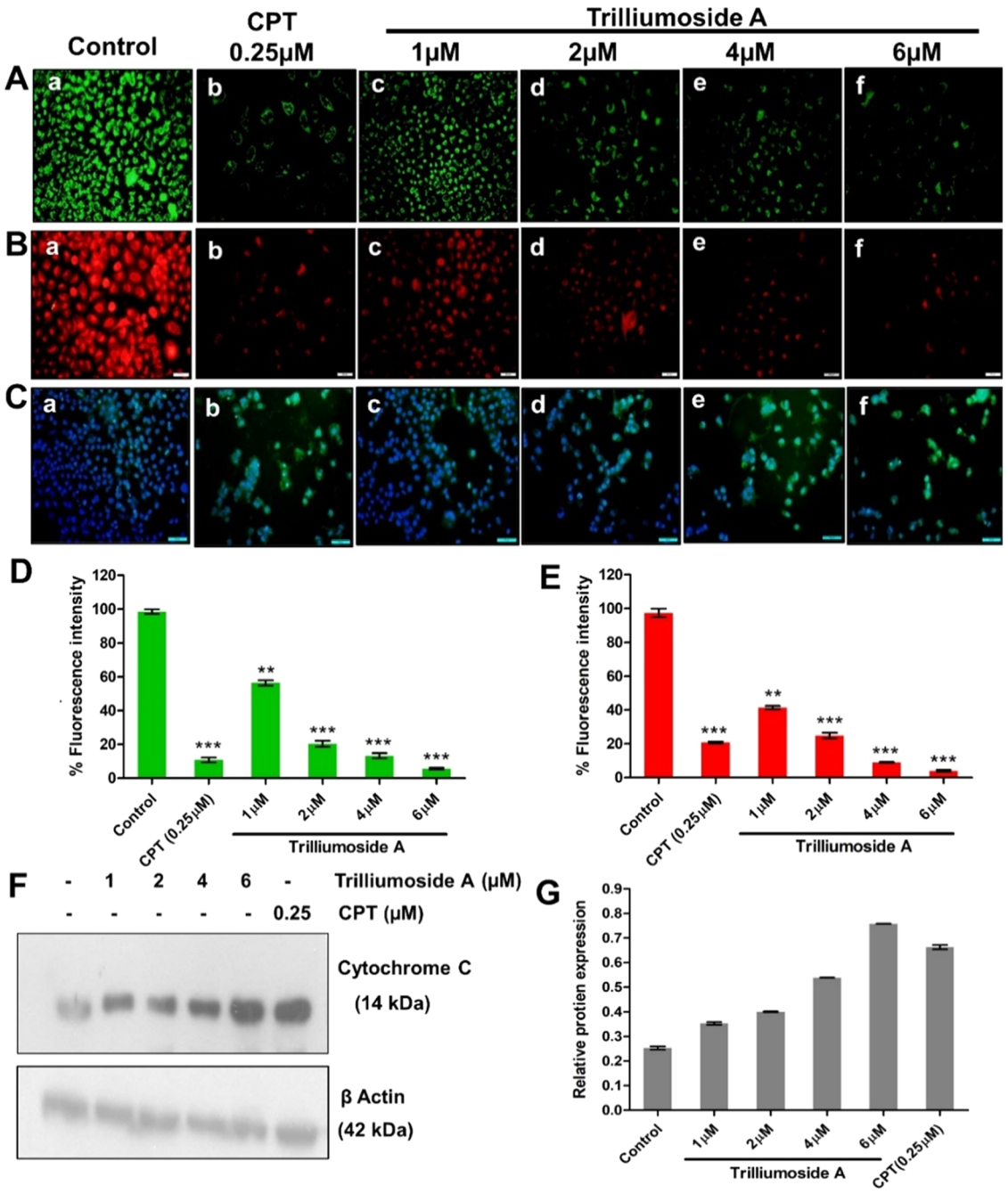

Figure 5. Trilliumoside A caused mitochondrial membrane depolarization in A549 cells. (A, D) Cells stained with Rhodamine 123 and (B, E) Mitotracker red dye. MMP loss was assessed using fluorescence microscopy upon treatment with Trilliumoside A at concentrations of 1, 2, 4, and 6 μM. The fluorescence intensity decreased with the increase in the concentration. CPT was used as a positive control. (C) Immunocytochemistry images depicting the release of cytochrome C at 48 h in A549 cells and fluorescence intensity increases with increasing concentration of Trilliumoside A. Secondary antibody used here is AlexaFlour 488 (green). (D, E) Bar graph showing the fluorescence intensity decreases as the concentration of Trilliumoside A increases. Data were expressed as mean ± SD, $^{**}P < 0.01$ and $^{***}P < 0.001$ represent significant differences as compared to the control. (F) Cytochrome C protein expression shows an increase in its expression in a concentration-dependent manner as analyzed by western blotting and (G) graph showing relative protein expression. Data were expressed as mean ± SD.

a loading control, β -actin was used. Bcl-2 family-associated protein expression was used to highlight the molecular mechanism of Trilliumoside A-induced apoptosis in A549 cells. As the Trilliumoside A concentration was increased, Bcl-2 was reduced, while the expression of pro-apoptotic proteins, including Bax, Bak, Bid, and Puma, appeared to be increased [Figure 7Ab, Ac and Bb, Bc].

3.14. Trilliumoside A Affects the p53/Mdm2 and Cyclin A/Cdk2 Complex Expression. The development of mechanism-driven anticancer therapies must focus on the tumor suppressor protein p53 since it is critical in the repair of DNA damage. For p53 to become activated upon DNA damage and apoptotic cell death, it must be phosphorylated. The most important site to investigate p53-dependent apoptosis induction is serine 46 phosphorylation of p53.

https://doi.org/10.1021/acsomega.3c03649
ACS Omega 2023, 8, 31914−31927

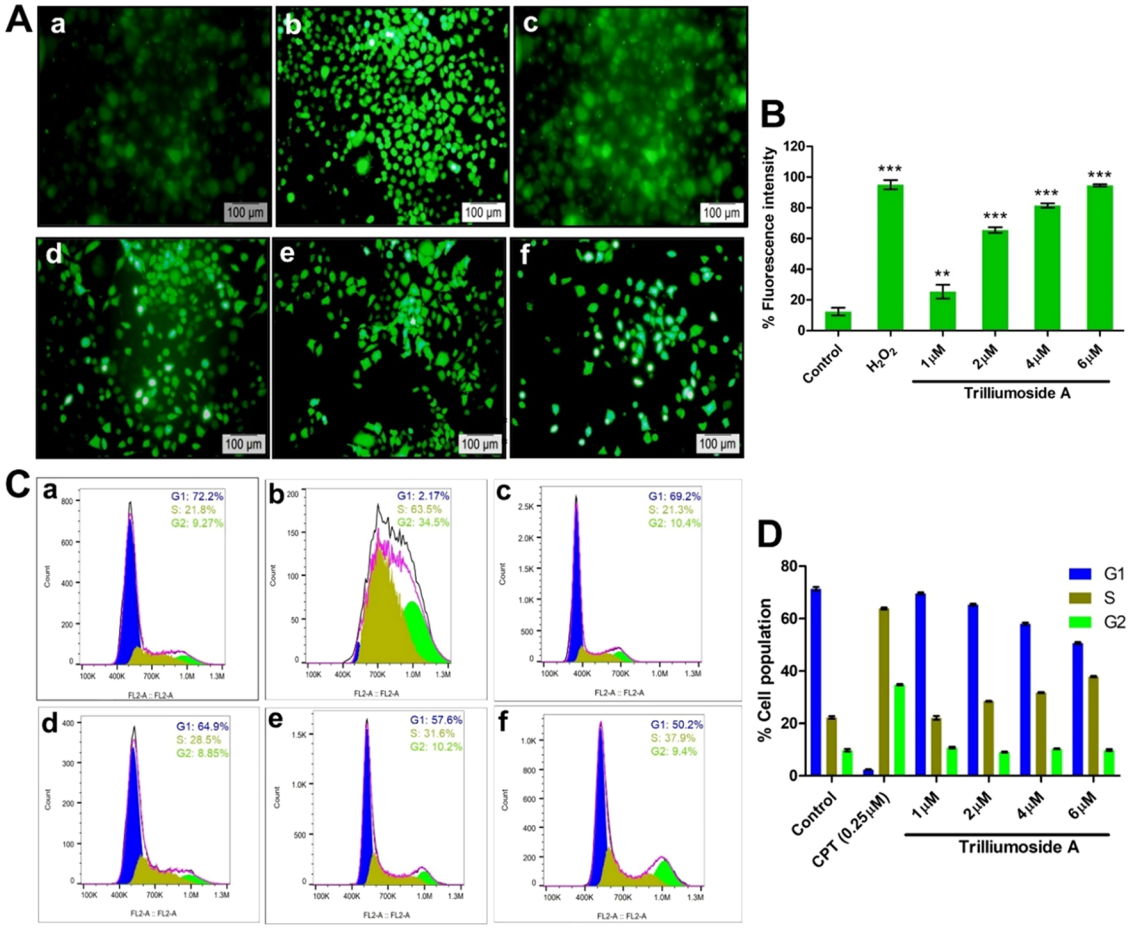

Figure 6. (A) Reactive oxygen species (ROS) are produced after treatment with Trilliumoside A. Trilliumoside A was incubated with A549 cells at various concentrations for 48 h to produce ROS. Fluorescence microscopy was used to measure the fluorescent intensity of the DCFH-DA dye. The fluorescence intensity increases with the increase in the concentration. H_2O_2 was used as a positive control. a–f indicate different groups, i.e., control, H_2O_2, Trilliumoside A (1 μM), Trilliumoside A (2 μM), Trilliumoside A (4 μM), and Trilliumoside A (6 μM), respectively, and (B) bar graph showing fluorescence intensity and data were denoted as mean ± SD, $^{**}P < 0.01$ and $^{***}P < 0.001$ represent significant difference as compared to the control. (C) Cell cycle arrest in Trilliumoside A-treated A549 cells. Following treatment with Trilliumoside for 48 h, the cell population distribution in the cell cycle was analyzed by flow cytometry after staining with the PI dye. Control, CPT (0.25 μM), Trilliumoside A (1 μM), Trilliumoside A (2 μM), Trilliumoside A (4 μM), and Trilliumoside A (6 μM) are denoted by a–f, respectively. (D) Histogram represents the quantification of cell cycle phase data. Data were expressed as mean ± SD.

Trilliumoside A was given to A549 cells at various dosages to see if p53 was phosphorylated at serine 46. Trilliumoside A increased the phosphorylation of p53 at site ser46 in a concentration-dependent manner, which increased p53 activity as shown in Figure 7Ad, Bd. As p53 is known to be negatively regulated by Mdm2 due to its ubiquitin ligase activity, the western blot results showed that pMdm2 is downregulated in response to Trilliumoside A in a concentration-dependent manner, maintaining the p53 function. We also used western blots to examine how Trilliumoside A therapy affected the concentration of proteins that control the cell cycle. In A549 cells treated with Trilliumoside A, cyclin A was downregulated, whereas p21 and p27 (CDK inhibitors) were upregulated in a concentration-dependent manner [Figure 7Ae, Af and Be, Bf]. These results demonstrate that Trilliumoside A treatment in A549 cells affects the S phase of the cell cycle.

3.15. In Vivo Studies on Trilliumoside A against Tumor Models. As in vitro investigations showed that Trilliumoside A triggered apoptosis in A549 cells; therefore, it was further tested for its in vivo anticancer effectiveness against murine tumor models.

3.15.1. Anticancer Efficacy of Trilliumoside A in Ehrlich Ascites Carcinoma (EAC). Trilliumoside A at doses of 25, 50, and 75 mg/kg (IP) was administered to EAC tumor-bearing mice for nine days in a row, and their responses were assessed on the twelfth day. 5-FU (20 mg/kg, IP) was employed as the positive control. In this ascitic tumor model, Trilliumoside A successfully reduced tumor growth. It showed a percent tumor growth inhibition of 39% at 25 mg/kg, 60% at 50 mg/kg, and 67.06% at 75 mg/kg dose in ehrlich ascites carcinoma (Figure 8A). Tumor cell count in animals treated with Trilliumoside A was lower than that of the saline-treated group of animals and thus exhibited significantly ($p < 0.001$) lower tumor growth. On day 12 of the experiment, 5-FU (positive controls) also exhibited significantly reduced tumor cell numbers in the treated animal peritoneal cavities.

3.15.2. Anticancer Activity against Ehrlich Tumor (Solid) Model. Trilliumoside A was administered in animals at doses of 50 and 75 mg/kg (IP) for nine consecutive days and evaluated on day 13 of the experiment. 5-FU (positive control) was given to one group at a dose of 22 mg/kg. Trilliumoside A inhibited the tumor growth in this murine solid tumor model

https://doi.org/10.1021/acsomega.3c03649
ACS Omega 2023, 8, 31914−31927

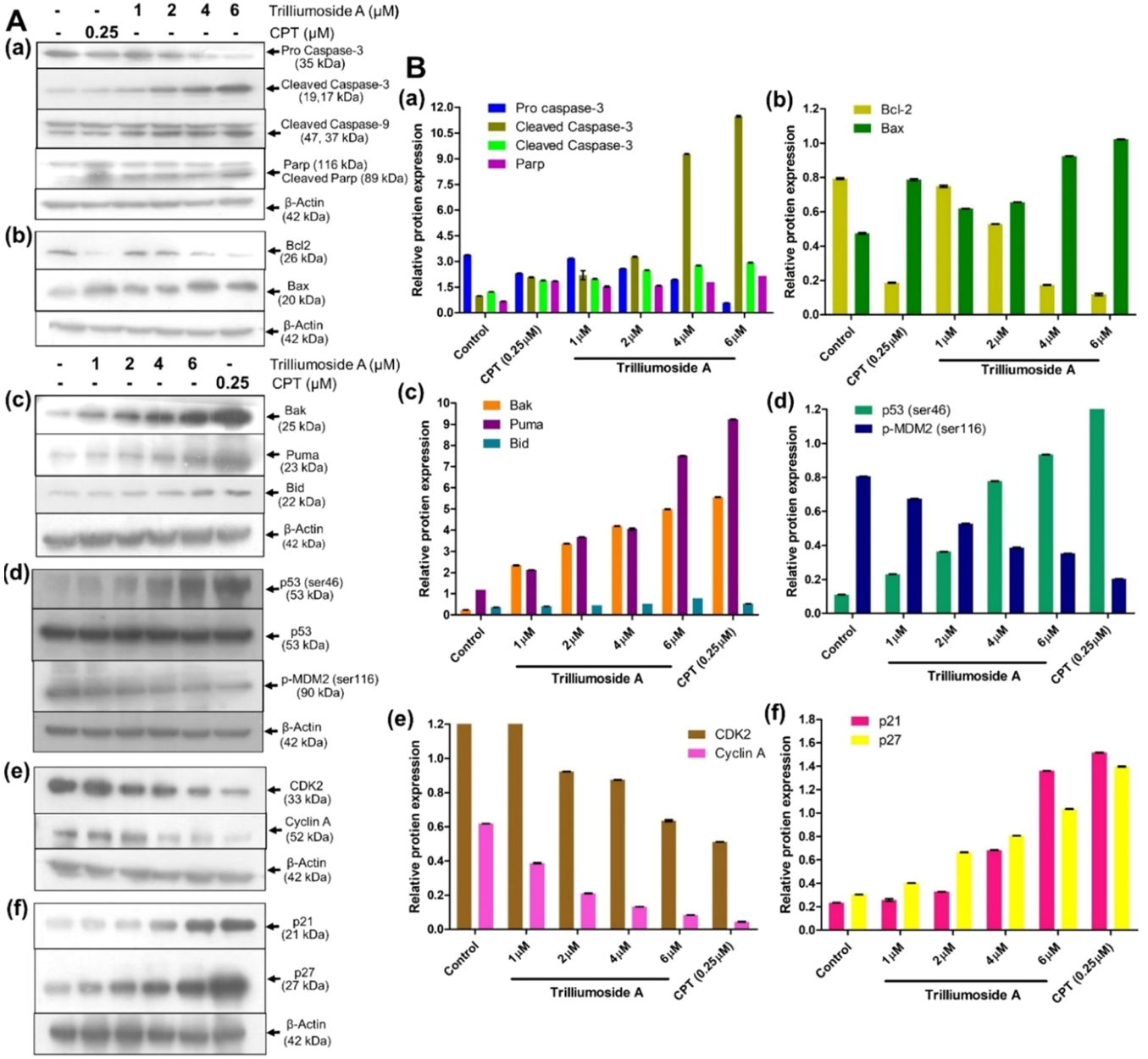

Figure 7. In A549 cells, Trilliumoside A induces cell death via an intrinsic pathway. (A) Western blot analysis and (B) bar graphs of protein expression of respective blots. Western blot analysis of apoptosis including various Caspases such as (a) cleaved caspase −3, 9, and PARP. (b, c) Trilliumoside A affects the expression of pro-apoptotic proteins, i.e., Bak and anti-apoptotic proteins like Bcl-2. Other pro-apoptotic proteins such as Bax, Puma, and Bid were analyzed. *β*-Actin was used as a loading control. (d) Western blot analysis demonstrated the increased expression of phosphorylated p53 and decreased expression of p-MDM2 compared to the negative control in cell lysates of A549 cells subjected to Trilliumoside A treatment for 48 h. (e) Expression of CDK2 and Cyclin A was decreased, whereas (f) there is an increase in the expression of CDK inhibitors such as p21 and p27, thereby confirming that in A549 cells, Trilliumoside A restricts the cell cycle in the S phase. Data were presented as mean ± SD.

and on the 13th day, 22.18 and 51.18% tumor growth inhibition was observed at 50 and 75 mg/kg, respectively. 5-FU at the 22 mg/kg dose level resulted in 68.19% tumor growth inhibition. The tumor growth inhibition by Trilliumoside A was significant ($p < 0.05$) at 75 mg/kg, and no mortality was observed in the Trilliumoside A treatment group (Figure 8B).

4. DISCUSSION

18.4% of all cancer-related deaths are caused by lung cancer, which is also the greatest cause of cancer-related mortality in women.[41] Although cutting-edge therapeutic approaches have been explored, patients with lung cancer still have a very bad prognosis. Clinicians and researchers have discovered over the past few decades that chemical compounds isolated from natural products may be helpful for treating lung cancer. For the treatment of lung cancer, drug formulations made from natural substances including paclitaxel, doxorubicin, and camptothecin have been effective. Through fundamental and subclinical research, hundreds of novel natural substances that can be utilized to treat lung cancer have been discovered in recent years. Nevertheless, there has not been a comparable

https://doi.org/10.1021/acsomega.3c03649
ACS Omega 2023, 8, 31914−31927

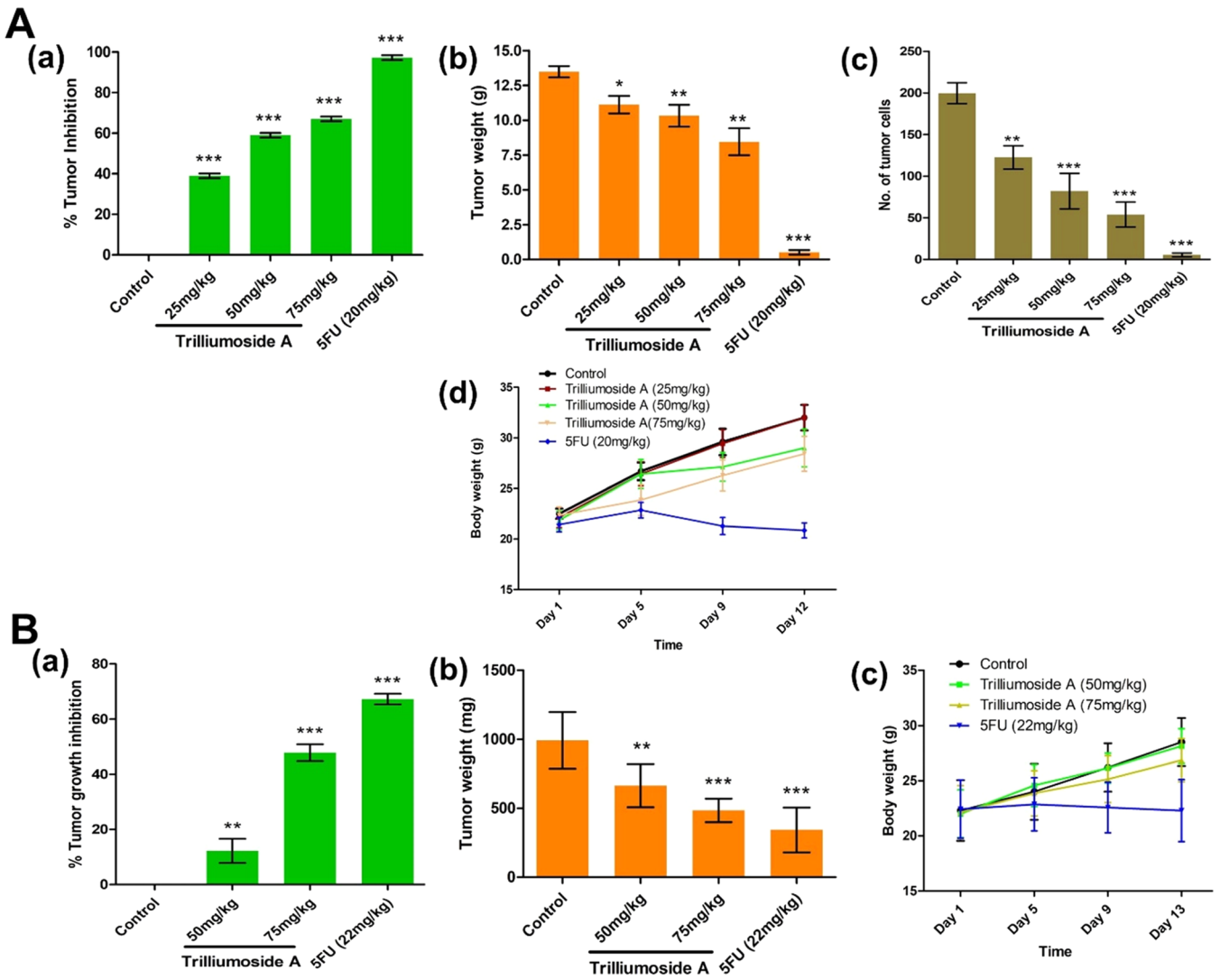

Figure 8. (A) Antitumor activity of Trilliumoside A against ehrlich ascites carcinoma (EAC) at different dose levels, i.e., 25, 50, and 75 mg/kg. The 5FU at 20 mg/kg dose was taken as a positive control. The bar graph shows (a) tumor growth was significantly inhibited in treatment groups as compared to the control group, reduced (b) tumor weight, and (c) a number of tumor cells were observed in treatment groups. (d) No significant reduction in body weight was obtained in treatment groups at different intervals. (B) Trilliumoside A's antitumor efficacy against ehrlich tumor (solid) was performed at various doses, i.e., 50 and 75 mg/kg. The 5FU at 22 mg/kg dose was taken as a positive control. The bar graph shows (a) tumor growth and (b) tumor weight significantly reduced in treatment groups as compared to the control group. (c) Body weight of different treatment groups at a fixed interval. Values are mean ± S.E. (n = 7, 10 for the control) *P < 0.05, **P < 0.01, and ***P < 0.001. Trilliumoside A-treated versus control (normal saline).

rise in the number of medications explored in clinical settings. Low solubility, restricted absorption, an unfavorable metabolism, and significant side effects are possible causes.

Plants have an ancient legacy of being used in cancer treatment. A study has reported nearly 3000 plant species that have anticancer properties.[42] The development of numerous anticancer medications currently being used in clinical settings is due to plant-based pharmaceuticals.[43] Vinca alkaloids, epipodophyllotoxin lignans, taxane, diterpenoids, steroidal saponins, and derivatives of camptothecin quinoline alkaloids make up the majority of the plant-based anticancer drugs. The genus *Trillium* yielded a large number of secondary metabolites. Terpenoids, sterols, flavonoids, saponin derivatives, and steroidal glycosides are only a few of the biologically active substances found in the genus.[44,45] Four human cancer cell lines—liver (HEPG2), breast (MCF7), lung (A549), and urinary bladder (EJ138)—show cytotoxic activity against the steroidal saponins found in the genus.[46]

Trilliumoside A, a naturally occurring chemical that was isolated from the rhizome of *T. govanianum*, exhibits excellent cytotoxicity against the A549 (lung cancer) cell line when tested against a panel of cancer cell lines. DAPI staining and ultrastructural observations through SEM revealed multiple abnormalities and morphological changes such as membrane blebbing, enlarged, flattened, and irregularly shaped cells with some projections in Trilliumoside A-treated cells as compared with untreated cells. To validate the apoptotic induction, AO/EtBr staining was done, which shows uniform green fluorescence by live cells and orange-red fluorescence in apoptotic and dead cells, respectively. The Annexin V FITC assay was used to further demonstrate Trilliumoside A's ability to cause apoptosis in A549 cells. The migration and clonogenic

https://doi.org/10.1021/acsomega.3c03649
ACS Omega 2023, 8, 31914−31927

potential of A549 cells also decreases as the concentration of Trilliumoside A was increased.

Trilliumoside A causes loss in mitochondrial membrane integrity that led to a significant loss of MMP, thereby confirming the release of cytochrome c. Reactive oxygen species (ROS) are mostly generated in the mitochondria of human cells, and ROS are frequently produced when MMP breaks down.[47] In A549 cells, Trilliumoside A causes MMP loss, thereby affecting the intracellular ROS level. Using the expression of Bcl-2 family-associated proteins, the molecular mechanism of Trilliumoside A-induced apoptosis in A549 cells was demonstrated.[48] Bcl-2 was reduced, but there was an increase the expression of pro-apoptotic proteins such as Bax, Bak, Bid, and Puma. Trilliumoside A-treated cells experience enhanced activity of caspases as the cleavage of caspase-3 and -9 got increased in a dose-dependent fashion, on comparison with control or untreated cells. Trilliumoside A activated PARP protein by cleaving it, initiating the cell death via intrinsic mode of apoptosis. Flow cytometric analysis was adopted to evaluate the DNA phase distribution[49] of A549 cells, and it was observed that Trilliumoside A inhibited cell cycle regulators of the S-phase.

The tumor suppressor protein p53 is essential in the repair of DNA damage and is a crucial target for mechanism-driven anticancer therapy development.[50] Phosphorylation of p53 is essential for activating p53 after DNA damage and apoptotic cell death. P53 phosphorylation at serine 46 is the leading site to explore p53-dependent apoptosis induction.[51] To find whether p53 is phosphorylated at serine 46, Trilliumoside A treatment was given to A549 cells at various doses. According to a Western blot examination of whole-cell lysates, Trilliumoside A boosted p53 activity by phosphorylating it at ser46 in a concentration-dependent manner. Due to Mdm2's ubiquitin ligase activity, which is known to be a negative regulator of p53, pMdm2 is downregulated in a concentration-dependent manner, which aids in maintaining the p53 function.[52] We also examined how Trilliumoside A therapy affected the concentration of proteins that control the cell cycle. Treatment with Trilliumoside A caused the CDK inhibitors p21 and p27 to be upregulated and Cyclin A to be downregulated in a concentration-dependent manner in A549 cells.[53] These findings showed that A549 cells on treatment with Trilliumoside A affect the S phase of the cell cycle. In vivo anticancer efficacy of Trilliumoside A was also tested against murine tumor models such as ehrlich ascites carcinoma and ehrlich tumor (solid). A considerable reduction in tumor volume, amount of ascitic fluid, and total cell number was observed without affecting the body weight of animals as compared to that of control group animals. No mortality was seen in animals at the administered doses.

5. CONCLUSIONS

In conclusion, our findings showed that Trilliumoside A inhibits the growth of A549 cells by inducing DNA damage, elevating the intracellular ROS level, by activating mitochondria-mediated apoptosis, and by arresting the cell cycle at the S-phase. Moreover, Trilliumoside A also showed notable tumor suppression without mortality in in vivo mouse tumor models. These findings support the potential of Trilliumoside A as a promising anticancer agent. The antitumor potential of Trilliumoside A in combination with the conventional anticancer agent would be of interest and requires further studies.

ASSOCIATED CONTENT

Supporting Information

The Supporting Information is available free of charge at https://pubs.acs.org/doi/10.1021/acsomega.3c03649.

Additional experimental details including the IC_{50} values of natural products against various human cancer cell lines, selectivity index, and time-dependent cytotoxicity of Trilliumoside A (PDF)

AUTHOR INFORMATION

Corresponding Authors

Dilip M. Mondhe − *Pharmacology Division, CSIR-Indian Institute of Integrative Medicine, Jammu 180001, India; Academy of Scientific and Innovative Research (AcSIR), Ghaziabad 201002, India*; Email: mondhe33@gmail.com

Prem N. Gupta − *Pharmacology Division, CSIR-Indian Institute of Integrative Medicine, Jammu 180001, India; Academy of Scientific and Innovative Research (AcSIR), Ghaziabad 201002, India*; orcid.org/0000-0003-3072-7000; Email: pngupta@iiim.res.in

Authors

Misbah Tabassum − *Pharmacology Division, CSIR-Indian Institute of Integrative Medicine, Jammu 180001, India; Academy of Scientific and Innovative Research (AcSIR), Ghaziabad 201002, India*

Bashir Ahmad Lone − *Natural Products and Medicinal Chemistry Division, CSIR-Indian Institute of Integrative Medicine, Jammu 180001, India; Academy of Scientific and Innovative Research (AcSIR), Ghaziabad 201002, India*

Mudasir Nazir Bhat − *Plant Science and Agrotechnology Division, CSIR-Indian Institute of Integrative Medicine, Jammu 180001, India; Academy of Scientific and Innovative Research (AcSIR), Ghaziabad 201002, India*

Anil Bhushan − *Natural Products and Medicinal Chemistry Division, CSIR-Indian Institute of Integrative Medicine, Jammu 180001, India; Academy of Scientific and Innovative Research (AcSIR), Ghaziabad 201002, India*

Nagma Banjare − *Pharmacology Division, CSIR-Indian Institute of Integrative Medicine, Jammu 180001, India; Academy of Scientific and Innovative Research (AcSIR), Ghaziabad 201002, India*

Esteban Manrique − *Real Jardin Botanico-CSIC, 28760 Madrid, Spain*

Prasoon Gupta − *Natural Products and Medicinal Chemistry Division, CSIR-Indian Institute of Integrative Medicine, Jammu 180001, India; Academy of Scientific and Innovative Research (AcSIR), Ghaziabad 201002, India*

Complete contact information is available at: https://pubs.acs.org/10.1021/acsomega.3c03649

Author Contributions

#M.T. and B.A.L. contributed equally.

Funding

This study was supported by the Indian Council of Medical Research, New Delhi (ICMR Grant no. 45/23/2022/TRM/BMS), and the University Grants Commission (GAP-1128).

Notes

The authors declare no competing financial interest.

■ ACKNOWLEDGMENTS

Misbah Tabassum acknowledges the University Grants Commission for Senior Research Fellowship (GAP-1128). Bashir Lone acknowledges the Indian Council of Medical Research (ICMR Grant no. 418 45/23/2022/TRM/BMS), New Delhi. The article is approved by the IPR committee (Institutional Publication number: CSIR-IIIM/IPR/00600). The authors thank the Director, CSIR-IIIM, Jammu, for infrastructure support.

■ REFERENCES

(1) de Martel, C.; Georges, D.; Bray, F.; Ferlay, J.; Clifford, G. M. Global burden of cancer attributable to infections in 2018: a worldwide incidence analysis. *Lancet Global Health* **2020**, *8*, e180−e190.

(2) Yang, D.; Liu, Y.; Bai, C.; Wang, X.; Powell, C. A. Epidemiology of lung cancer and lung cancer screening programs in China and the United States. *Cancer Lett.* **2020**, *468*, 82−87.

(3) Ramalingam, S. S.; Owonikoko, T. K.; Khuri, F. R. Lung cancer: New biological insights and recent therapeutic advances. *CA Cancer J. Clin.* **2011**, *61*, 91−112.

(4) Mathers, C. D.; Shibuya, K.; Boschi-pinto, C.; Lopez, A. D.; Murray, C. J. L. Global and regional estimates of cancer mortality and incidence by cancer mortality distribution by site. *BMC Cancer* **2002**, *2*, 1471−2407.

(5) Depciuch, J.; Klębowski, B.; Stec, M.; Szatanek, R.; Węglarczyk, K.; Baj-krzyworzeka, M.; Parlińska-wojtan, M.; Baran, J. Similarities in the general chemical composition of colon cancer cells and their microvesicles investigated by spectroscopic methods-potential clinical relevance. *Int. J. Mol. Sci.* **2020**, *21*, No. 1826.

(6) Parkin, D. M.; Bray, F.; Ferlay, J.; Pisani, P. Global cancer statistics, 2002. *Ca-Cancer J. Clin.* **2005**, *55*, 74−108.

(7) Potiron, V. A.; Roche, J.; Drabkin, H. A. Semaphorins and their receptors in lung cancer. *Cancer Lett.* **2009**, *273*, 1−14.

(8) Rawla, P.; Sunkara, T.; Barsouk, A. Epidemiology of colorectal cancer: Incidence, mortality, survival, and risk factors. *Gastroenterol. Rev.* **2019**, *14*, 89−103.

(9) Markou, A.; Zavridou, M.; Lianidou, E. S. miRNA-21 as a novel therapeutic target in lung cancer. *Lung Cancer: Targets Ther.* **2016**, *7*, 19−27.

(10) Cory, S.; Adams, J. M. The BCL2 family: Regulators of the cellular life-or-death switch. *Nat. Rev. Cancer* **2002**, *2*, 647−656.

(11) Everett, H.; McFadden, G. Viruses and apoptosis: Meddling with mitochondria. *Virology* **2001**, *288*, 1−7.

(12) Rathore, S.; Walia, S.; Devi, R.; Kumar, R. Review on Trillium govanianum Wall. ex D. Don: A threatened medicinal plant from the Himalaya. *J. Herb. Med.* **2020**, *24*, No. 100395.

(13) Roa, W. H.; Azarmi, S.; Al-Hallak, M. H. D. K.; Finlay, W. H.; Magliocco, A. M.; Löbenberg, R. Inhalable nanoparticles, a non-invasive approach to treat lung cancer in a mouse model. *J. Controlled Release* **2011**, *150*, 49−55.

(14) Lu, J.; Liong, M.; Zink, J. I.; Tamanoi, F. Mesoporous silica nanoparticles as a delivery system for hydrophobic anticancer drugs. *Small.* **2007**, *3*, 1341−1346.

(15) Kumar, A.; Sahoo, S. K.; Padhee, K.; Kochar, P. S.; Sathapathy, A.; Pathak, N. Review on solubility enhancement techniques for hydrophobic drugs. *Pharm. Globale* **2011**, *3*, 001−007.

(16) Tseng, C. L.; Wu, S. Y. H.; Wang, W. H.; Peng, C. L.; Lin, F. H.; Lin, C. C.; Young, T. H.; Shieh, M. J. Targeting efficiency and biodistribution of biotinylated-EGF-conjugated gelatin nanoparticles administered via aerosol delivery in nude mice with lung cancer. *Biomaterials* **2008**, *29*, 3014−3022.

(17) Mintoo, M.; Khan, S.; Wani, A.; Malik, S.; Bhurta, D.; Bharate, S.; Malik, F.; Mondhe, D. A rohitukine derivative IIIM-290 induces p53 dependent mitochondrial apoptosis in acute lymphoblastic leukemia cells. *Mol. Carcinog.* **2021**, *60*, 671−683.

(18) Force, T.; Kerkelä, R. Cardiotoxicity of the new cancer therapeutics - mechanisms of, and approaches to, the problem. *Drug Discovery Today* **2008**, *13*, 778−784.

(19) Russo, P. Cardiac toxicity of sunitinib and sorafenib in patients with metastatic renal cell carcinoma. *Urol. Oncol.: Semin. Orig. Invest.* **2009**, *27*, 103−104.

(20) Lichota, A.; Gwozdzinski, K. Anticancer activity of natural compounds from plant and marine environment. *Int. J. Mol. Sci.* **2018**, *19*, No. 3533.

(21) Chekem, L.; Wierucki, S. Extraction de l'artémisinine et synthèse de ses dérivés artésunate et artéméther. *Méd. Trop* **2006**, *66*, 602−605.

(22) Bocca, C. Taxol: A short history of a promising anticancer drug. *Minerva Biotecnol.* **1998**, *10*, 81.

(23) Gupta, P.; Lone, B. A.; Tabassum, M.; Bhushan, A.; Dhiman, U.; Rani, D.; Gairola, S.et al. Trilliumosides AB, two novel steroidal saponins isolated from Rhizomes of Trillium govanianum as potent anticancer agents targeting apoptosis in A-549 cancer cell line*bioRxiv* p 2023 DOI: 10.1101/2023.04.17.537170.

(24) Luo, Q.; Li, Z.; Huang, X.; Yan, J.; Zhang, S.; Cai, Y. Z. Lycium barbarum polysaccharides: Protective effects against heat-induced damage of rat testes and H2O2-induced DNA damage in mouse testicular cells and beneficial effect on sexual behavior and reproductive function of hemicastrated rats. *Life Sci.* **2006**, *79*, 613−621.

(25) Wang, H.; Zhai, Z.; Li, N.; Jin, H.; Chen, J.; Yuan, S.; Wang, L.; Zhang, J.; Li, Y.; Yun, J.; Fan, J.; Yi, J.; Ling, R. Steroidal saponin of Trillium tschonoskii. Reverses multidrug resistance of hepatocellular carcinoma. *Phytomedicine* **2013**, *20*, 985−991.

(26) Segeritz, C. P.; Vallier, L. Cell Culture: Growing Cells as Model Systems In Vitro. In *Basic Science Methods for Clinical Researchers*; Academic Press, 2017; pp 151−172.

(27) Vichai, V.; Kirtikara, K. Sulforhodamine B colorimetric assay for cytotoxicity screening. *Nat. Protoc.* **2006**, *1*, 1112−1116.

(28) Atale, N.; Gupta, S.; Yadav, U. C. S.; Rani, V. Cell-death assessment by fluorescent and nonfluorescent cytosolic and nuclear staining techniques. *J. Microsc.* **2014**, *255*, 7−19.

(29) Bharate, S. B.; Kumar, V.; Jain, S. K.; Mintoo, M. J.; Guru, S. K.; Nuthakki, V. K.; Vishwakarma, R. A.; et al. Discovery and preclinical development of IIIM-290, an orally active potent cyclin-dependent kinase inhibitor. *J. Med. Chem.* **2018**, *61*, 1664−1687.

(30) Nanayakkara, A. K.; Follit, C. A.; Chen, G.; Williams, N. S.; Vogel, P. D.; Wise, J. G. Targeted inhibitors of P-glycoprotein increase chemotherapeutic-induced mortality of multidrug resistant tumor cells. *Sci. Rep.* **2018**, *8*, No. 967.

(31) Majeed, R.; Hamid, A.; Sangwan, P. L.; Chinthakindi, P. K.; Koul, S.; Rayees, S.; Saxena, A. K.; et al. Inhibition of phosphotidylinositol-3 kinase pathway by a novel naphthol derivative of betulinic acid induces cell cycle arrest and apoptosis in cancer cells of different origin. *Cell Death Dis.* **2014**, *5*, e1459.

(32) Hua, R.; Pei, Y.; Gu, H.; Sun, Y.; He, Y. Antitumor effects of flavokawain-B flavonoid in gemcitabine-resistant lung cancer cells are mediated via mitochondrial-mediated apoptosis, ROS production, cell migration and cell invasion inhibition and blocking of PI3K/AKT Signaling pathway. *J. Buon* **2020**, *25*, 262−267.

(33) Gupta, N.; Qayum, A.; Raina, A.; Shankar, R.; Gairola, S.; Singh, S.; Sangwan, P. L. Synthesis and biological evaluation of novel bavachininanalogs as anticancer agents. *Eur. J. Med. Chem.* **2018**, *145*, 511−523.

(34) Kumar, A.; Singh, B.; Mahajan, G.; Sharma, P. R.; Bharate, S. B.; Mintoo, M. J.; Mondhe, D. M. A novel colchicine-based microtubule inhibitor exhibits potent antitumor activity by inducing mitochondrial mediated apoptosis in MIA PaCa-2 pancreatic cancer cells. *Tumor Biol.* **2016**, *37*, 13121−13136.

(35) Wani, A.; Gupta, M.; Ahmad, M.; Shah, A. M.; Ahsan, A. U.; Qazi, P. H.; Kumar, A.; et al. Alborixin clears amyloid-β by inducing autophagy through PTEN-mediated inhibition of the AKT pathway. *Autophagy* **2019**, *15*, 1810−1828.

https://doi.org/10.1021/acsomega.3c03649
ACS Omega 2023, 8, 31914−31927

(36) Shankar, S.; Faheem, M. M.; Nayak, D.; Wani, N. A.; Farooq, S.; Koul, S.; Goswami, A.; Rai, R. Cyclodipeptide c (orn-pro) conjugate with 4-ethylpiperic acid abrogates cancer cell metastasis through modulating mdm2. *Bioconjugate Chem.* **2018**, *29*, 164−175.
(37) Bhushan, S.; Kumar, A.; Malik, F.; Andotra, S. S.; Sethi, V. K.; Kaur, I. P.; Singh, J. A.; et al. triterpenediol from Boswellia serrata induces apoptosis through both the intrinsic and extrinsic apoptotic pathways in human leukemia HL-60 cells. *Apoptosis* **2007**, *12*, 1911−1926.
(38) Yu, Z.; Li, W. Induction of apoptosis by puerarin in colon cancer HT-29 cells. *Cancer Lett.* **2006**, *238*, 53−60.
(39) Hussain, A.; Qazi, A. K.; Mupparapu, N.; Kumar, A.; Mintoo, M. J.; Mahajan, G.; Hamid, A.; et al. A novel PI3K axis selective molecule exhibits potent tumor inhibition in colorectal carcinogenesis. *Mol.Carcinog.* **2016**, *55*, 2135−2155.
(40) Singh, B.; Kumar, A.; Joshi, P.; Guru, S. K.; Kumar, S.; Wani, Z. A.; Vishwakarma, R. A.; et al. Colchicine derivatives with potent anticancer activity and reduced P-glycoprotein induction liability. *Org. Biomol. Chem.* **2015**, *13*, 5674−5689.
(41) Wen, T.; Song, L.; Hua, S. Perspectives and controversies regarding the use of natural products for the treatment of lung cancer. *Cancer Med.* **2021**, *10*, 2396−2422.
(42) Kluwe, W. M.; McConnell, E. E.; Huff, J. E.; Haseman, J. K.; Douglas, J. F.; Hartwell, W. V. Carcinogenicity testing of phthalate esters and related compounds by the National Toxicology Program and the National Cancer Institute. *Environ. Health Perspect.* **1982**, *45*, 129−133.
(43) Hirschfeld, R. M.; Klerman, G. L.; Clayton, P. J.; Keller, M. B.; McDonald-Scott, P.; Larkin, B. H. Assessing personality: effects of the depressive state on trait measurement. *Am. J. Psychiatry* **1983**, *140*, 695−699.
(44) Hayes, P. Y.; Lehmann, R.; Penman, K.; Kitching, W.; De Voss, J. J. Steroidal saponins from the roots of Trillium erectum (Beth root). *Phytochemistry* **2009**, *70*, 105−113.
(45) Yoshitama, K.; Oyamada, T.; Yahara, S. Flavonoids in the leaves of Trillium undulatum Willdenow. *J. Plant Res.* **1997**, *110*, 379−381.
(46) Khan, K. M.; Nahar, L.; Al-Groshi, A.; Zavoianu, A. G.; Evans, A.; Dempster, N. M.; Sarker, S. D.; et al. Cytotoxicity of the roots of Trillium govanianum against breast (MCF7), liver (HepG2), lung (A549) and urinary bladder (EJ138) carcinoma cells. *Phytother. Res.* **2016**, *30*, 1716−1720.
(47) Szatrowski, T. P.; Nathan, C. F. Production of large amounts of hydrogen peroxide by human tumor cells. *Cancer Res.* **1991**, *51*, 794−798.
(48) POREBSKA, I.; Wyrodek, E.; Kosacka, M.; Adamiak, J.; Jankowska, R.; Harłozińska-Szmyrka, A. Apoptotic markers p53, Bcl-2 and Bax in primary lung cancer. *In Vivo* **2006**, *20*, 599−604.
(49) Nunez, R. DNA measurement and cell cycle analysis by flow cytometry. *Curr. Issues Mol. Biol.* **2001**, *3*, 67−70.
(50) Valente, J. F.; Queiroz, J. A.; Sousa, F. p53 as the focus of gene therapy: past, present and future. *Curr. Drug Targets* **2018**, *19*, 1801−1817.
(51) Smeenk, L.; van Heeringen, S. J.; Koeppel, M.; Gilbert, B.; Janssen-Megens, E.; Stunnenberg, H. G.; Lohrum, M. Role of p53 serine 46 in p53 target gene regulation. *PloS One* **2011**, *6*, No. e17574.
(52) Wu, H.; Leng, R. P. UBE4B, a ubiquitin chain assembly factor, is required for MDM2-mediated p53 polyubiquitination and degradation. *Cell Cycle* **2011**, *10*, 1912−1915.
(53) Abukhdeir, A. M.; Park, B. H. P21 and p27: roles in carcinogenesis and drug resistance. *Expert Rev. Mol. Med.* **2008**, *10*, No. e19.

https://doi.org/10.1021/acsomega.3c03649
ACS Omega 2023, 8, 31914−31927